An Isolated White Dwarf with a 70 s Spin Period

Mukremin Kilic[1] , Alekzander Kosakowski[2] , Adam G. Moss[1] , P. Bergeron[3] , and Annamarie A. Conly[1]
[1] Homer L. Dodge Department of Physics and Astronomy, University of Oklahoma, 440 W. Brooks St., Norman, OK, 73019 USA
[2] Department of Physics and Astronomy, Texas Tech University, Lubbock, TX 79409, USA
[3] Département de Physique, Université de Montréal, C.P. 6128, Succ. Centre-Ville, Montréal, Quebec H3C 3J7, Canada
Received 2021 October 15; revised 2021 November 10; accepted 2021 November 19; published 2021 December 7

Abstract

We report the discovery of an isolated white dwarf with a spin period of 70 s. We obtained high-speed photometry of three ultramassive white dwarfs within 100 pc and discovered significant variability in one. SDSS J221141.80 +113604.4 is a 1.27 $M_\odot$ (assuming a CO core) magnetic white dwarf that shows 2.9% brightness variations in the BG40 filter with a 70.32 ± 0.04 s period, becoming the fastest spinning isolated white dwarf currently known. A detailed model atmosphere analysis shows that it has a mixed hydrogen and helium atmosphere with a dipole field strength of $B_d = 15$ MG. Given its large mass, fast rotation, strong magnetic field, unusual atmospheric composition, and relatively large tangential velocity for its cooling age, J2211+1136 displays all of the signatures of a double white dwarf merger remnant. Long-term monitoring of the spin evolution of J2211+1136 and other fast-spinning isolated white dwarfs opens a new discovery space for substellar and planetary mass companions around white dwarfs. In addition, the discovery of such fast rotators outside of the ZZ Ceti instability strip suggests that some should also exist within the strip. Hence, some of the monoperiodic variables found within the instability strip may be fast-spinning white dwarfs impersonating ZZ Ceti pulsators.

Unified Astronomy Thesaurus concepts: Magnetic variable stars (996); White dwarf stars (1799); Compact objects (288); Stellar remnants (1627); Periodic variable stars (1213); Short period variable stars (1453)

1. Introduction

Angular momentum transport between the core and the envelope should slow the rotation of the core during the giant branch evolution, leading to the formation of slowly rotating white dwarfs (Kawaler 2004; Tayar & Pinsonneault 2013). Measurement of the white dwarf rotation rate is possible through high cadence observations of pulsating or spotted white dwarfs, or high-resolution spectroscopy of the NLTE Hα core in DA white dwarfs. The latter indicates no or very slow rotation in the majority of the observed systems, with typical lower limits of hours or longer rotation periods (Koester et al. 1998).

Asteroseismology of isolated pulsating white dwarfs confirm these findings; average-mass white dwarfs with $M = 0.51$–0.73 $M_\odot$ have a mean rotation period of 35 ± 28 hr (Kawaler 2015; Hermes et al. 2017b). Hermes et al. (2017b) discuss a possible link between white dwarf mass and rotation rate. There are three massive pulsating white dwarfs in their sample with $M = 0.78$–0.88 $M_\odot$ and those show significantly faster rotation rates of 1.1–8.9 hr (see also Hermes et al. 2017a).

Magnetic white dwarfs tend to spin faster than their nonmagnetic counterparts. Brinkworth et al. (2013) found photometric variability in 67% of the isolated magnetic white dwarfs in their sample, with periods ranging from 27 minutes to 6 days, plus two additional longer period systems. They also found no correlation between spin period and any other white dwarf parameters, including mass.

Kawka (2020) and Ferrario et al. (2020) presented a summary of the rotation period measurements for magnetic white dwarfs: most have rotation periods shorter than 10 hr,

with a distribution that peaks at 2–3 hr. Some of the fastest rotators are hot DQ white dwarfs with rotation periods as short as 5 minutes (Montgomery et al. 2008; Dufour et al. 2011; Williams et al. 2016). The combination of fast rotation rates, unique chemical composition, high mass, and high incidence of magnetism in hot DQ white dwarfs favor a double white dwarf merger origin for the formation of these stars (Dunlap & Clemens 2015; Coutu et al. 2019).

Kilic et al. (2021) presented an analysis of the ultramassive ($M \geqslant 1.3 M_\odot$) white dwarf candidates in the Montreal White Dwarf Database (MWDD, Dufour et al. 2017) 100 pc sample, and identified four outliers in transverse velocity, four likely magnetic white dwarfs (one of which is also an outlier in transverse velocity), and one with rapid rotation. They concluded that at least 32% of the 25 ultramassive white dwarfs in that sample are likely double white dwarf merger products. Among these ultramassive white dwarfs, J183202.83+085636.24 was previously identified as a rapid rotator with a spin period of 353 s (Pshirkov et al. 2020). Recently, Caiazzo et al. (2021) found a rotation period of 6.94 minutes in another of these objects, J190132.9+145808.7, based on photometric variability detected in the Zwicky Transient Facility (Bellm et al. 2019). These rotation rates are consistent with the theoretical predictions for single white dwarfs that formed from double white dwarf mergers (Schwab 2021).

There are three additional confirmed or suspected magnetic white dwarfs known in the Kilic et al. (2021) ultramassive white dwarf sample; SDSS J221141.80+113604.5 is a DAH with weak Hα and Hβ features, SDSS J225513.48+071000.9 has a DC-like spectrum that shows broad unidentified features, and WD J010338.56−052251.96 (G270-126) is a DAH: (Tremblay et al. 2020). We refer to these systems as J2211 +1136, J2255+0710, and J0103−0522, respectively. We obtained follow-up high-speed time-series photometry of these three systems to constrain their rotation rates. Table 1 presents
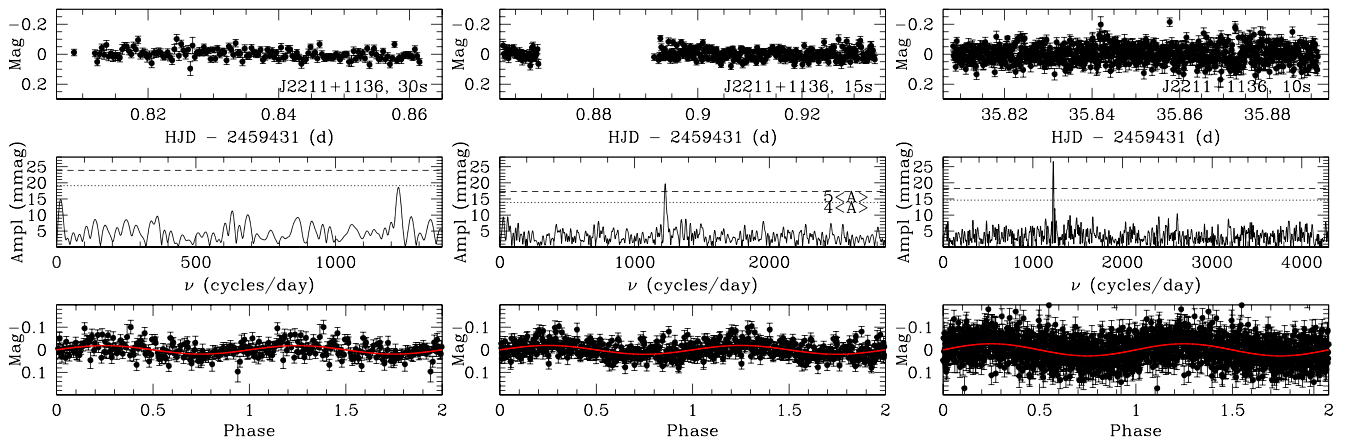
Figure 1. Top panels: APO time-series photometry of J2211+1136 based on 30 (left), 15 (middle), and 10 s long exposures (right). Middle panels: Fourier transform of each light curve. The dotted and dashed lines show the $4\langle A\rangle$ and $5\langle A\rangle$ levels, where $\langle A\rangle$ is the average amplitude in the Fourier transform. Bottom panels: The same light curves folded at the highest peak in the Fourier transform, along with the best-fitting sinusoidal model (red line).

Table 1
Details of APO 3.5 m Agile Observations

Object	Gaia DR2 Source ID	g (mag)	Exposures	UT Date
SDSS J221141.80+113604.5	2727596187657230592	19.28	145×30 s, 281×15 s	2021 Aug 5
⋯	⋯	⋯	720×10 s	2021 Sep 9
SDSS J225513.48+071000.9	2712093451662656256	19.15	181×15 s	2021 Aug 5
WD J010338.56−052251.96	2524879812959998592	17.41	1440×5 s	2021 Sep 9

the details of our observations for each target. We present the light curves for J2211+1136 in Section 2, those for J2255+0710 and J0103−0522 in Section 3, discuss the variability in J2211+1136 and its implications in Section 4, and conclude in Section 5.

2. J2211+1136

2.1. Photometric Variability

We acquired high-speed photometry of J2211+1136 over 76 minutes on UT 2021 August 5 using the APO 3.5 m telescope with the Agile frame transfer camera and the BG40 filter. We obtained 30 s long back-to-back exposures and binned the CCD by 2×2, which resulted in a plate scale of $0''\!.258$ pixel^{-1}.

A quick reduction of these data soon after acquisition revealed a frequency peak near 70 s, which was barely resolved due to our 30 s long exposures. To improve our time resolution, we decreased the exposure time to 15 s, and obtained an additional set of 281 exposures on the same night. Our efforts to re-observe J2211+1136 on August 13 and September 1 failed due to the monsoon season, but we were finally able to obtain 2 hr of 10 s long back-to-back exposures on UT 2021 September 9 under clear skies and subarcsecond seeing.

Figure 1 shows these light curves based on 30 (left), 15 (middle), and 10 s (right) long exposures. The middle panels show the Fourier transform of each data set. All three data sets show a single peak around 70 s in Fourier space, which is detected at the $\langle 4A\rangle$ level in the 30 s cadence data and above the $\langle 5A\rangle$ level in the higher-cadence data. The bottom panels show each light curve folded at the highest peak in the Fourier transform along with the best-fitting sinusoidal model (red line).

Treating the 30, 15, and 10 s data sets separately, the former indicates 19 ± 3 millimag variations with $P = 70.45 \pm 0.12$ s,

whereas the second data set indicates 20 ± 3 millimag variations with $P = 70.39 \pm 0.06$ s. The higher-cadence September 9 data set (right panels) shows a larger peak in its Fourier transform at $\nu = 1228.7 \pm 0.7$ cycles day^{-1}, or $P = 70.32 \pm 0.04$ s, with a 27 ± 3 millimag amplitude. The period estimates from these three different data sets with 30, 15, and 10 s exposures agree within the errors. Since the latter data set has the longest baseline and highest cadence, it provides the best constraints on the period and amplitude of the observed variations. Even then, because our 10 s exposures span 14.2% of the rotation phase ($\delta\phi = 0.89$ radians), the observed amplitude is underestimated by a factor of $\sin\delta\phi/\delta\phi = 0.87$. The true amplitude of variability is thus 31 millimag, or 2.9%.

2.2. Model Atmosphere Analysis

We computed magnetic model spectra using an approach similar to that described in Bergeron et al. (1992), where the line displacements and strengths of the Zeeman components are taken from the tables of Kemic (1974), with the exception that here we include Hα through Hδ. In addition to resonance broadening by neutral hydrogen, and van der Waals broadening by neutral hydrogen and helium (included following the prescription of Bergeron et al. 1997), we also take into account Stark broadening, which dominates the broadening of higher Balmer lines at the temperature of the object studied here. The total line opacity can be expressed as the sum of the individual Stark-, resonance-, and van-der-Waals-broadened Zeeman components.

The specific intensities at the surface, $I(\nu, \mu, \tau_\nu = 0)$, are obtained by solving the radiative transfer equation for various field strengths and values of μ ($\mu = \cos\theta$, where θ is the angle between the angle of propagation of light and the normal to the surface of the star). Finally, the emergent spectrum is obtained
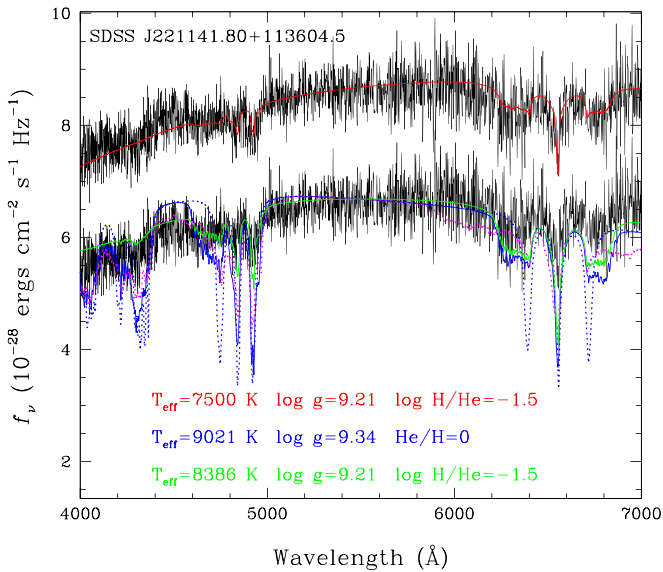
Figure 2. Our best fits to the SDSS spectrum of the magnetic DA white dwarf J2211+1136. The lower fits are for synthetic spectra calculated at temperatures and surface gravities determined from photometric fits under the assumption of a pure hydrogen composition (solid blue) and a mixed composition of log H/He = −1.5 (solid green), a dipole field strength of B_d = 15 MG, a centered dipole ($a_z = 0$), and a viewing angle of $i = 45°$. All spectra are normalized at 5500 Å. For comparison, we also show the offset dipole models for the pure H solution with $a_z = -0.2$ and $+0.2$ as dotted blue (with very sharp Zeeman components) and magenta lines, respectively. The optical spectrum is reproduced at the top of the figure, arbitrarily shifted vertically for clarity, and compared with a model spectrum where the effective temperature for the mixed H/He solution is decreased to $T_{eff} = 7500$ K.

from an integration over the surface of the star ($H_\nu \propto \int I_\nu \mu\, d\mu$) for a particular geometry of the magnetic-field distribution. Here we consider the same offset dipole model described in Bergeron et al. (1992), where the independent parameters are the dipole field strength B_d, the dipole offset a_z measured in units of stellar radius from the center of the star, and the viewing angle i between the dipole axis and the line of sight ($i = 0°$ for a pole-on view).

We first assume that J2211+1136 has a pure hydrogen composition and measure its effective temperature and stellar radius by fitting the available SDSS u and Pan-STARRS *grizy* photometry along with the Gaia EDR3 parallax. Details of our fitting procedure, model atmosphere grid (including models with mixed H/He compositions), as well as the evolutionary models used to derive the stellar mass and surface gravity, are described in Kilic et al. (2020) and references therein. The best-fitting model under the assumption of a pure hydrogen composition has $T_{eff} = 9021 \pm 160$ K, $M = 1.312 \pm 0.010\ M_\odot$, and $\log g = 9.338 \pm 0.030$. However, a pure hydrogen composition is clearly ruled out since the higher Balmer lines are predicted way too strong, no matter the assumed field strength and geometry. Figure 2 shows our magnetic model fits to the SDSS spectrum of J2211+1136, including the pure hydrogen atmosphere solution (solid blue line). Here we simply assumed a dipole field strength of $B_d = 15$ MG, a centered dipole ($a_z = 0$), and a viewing angle of $i = 45°$, which are the values obtained for our best fit with a mixed H/He composition discussed in the next paragraph. For comparison, we also show the offset dipole models with $a_z = -0.2$ and $+0.2$ as dotted blue and magenta lines, respectively. Even though offset dipole models are commonly used in modeling magnetic white dwarfs (e.g., Rolland & Bergeron 2015), a centered dipole clearly

provides a better fit to the observed line profiles in J2211+1136.

One obvious way to reduce the strength of the higher-order Balmer lines is to assume that the star has a mixed H and He composition (see, e.g., Figure 13 of Bergeron et al. 1991). Such He-rich DA stars have been identified in large numbers in the SDSS (Rolland et al. 2018). We therefore refitted the photometric energy distribution, this time assuming various values of the hydrogen-to-helium abundance ratio in number, H/He. We then explored different values of the field strength and offset for each solution and considered two viewing angles, $i = 45°$ and $60°$. We also explored rotational broadening and found that it only affects the line core. Our best overall fit, shown in green in Figure 2, is achieved with a mixed composition of log H/He = −1.5, from which we measure $T_{eff} = 8386 \pm 267$ K, $M = 1.268 \pm 0.010\ M_\odot$, and $\log g = 9.214 \pm 0.027$, for the same field geometry as above ($B_d = 15$ MG, $a_z = 0$, and $i = 45°$).

Clearly, the mixed H/He solution provides a much better fit to the optical spectrum of J2211+1136 than the pure hydrogen model. However, both the strength of Hα and the slope of the energy distribution suggest a lower temperature. We arbitrarily lowered the effective temperature of the mixed H/He solution to $T_{eff} = 7500$ K, and found that this model provides an excellent fit to the optical spectrum. This solution is displayed in red in Figure 2.

There are likely two reasons for the significant temperature difference between the photometric and spectroscopic solutions. First, the SDSS spectrum of J2211+1136 is a combination of eight subexposures with a total exposure time of 7207 s; it covers more than 100 rotation periods (see Section 4.1). Hence, any spectral changes due the magnetic-field geometry or surface inhomogeneities would lead to additional smearing of the Zeeman split lines in the combined SDSS spectrum. Second, Külebi et al. (2009) noted that no atomic data for hydrogen in the presence of both a magnetic and electric field are available for arbitrary strengths and arbitrary angles between two fields. Therefore, there may be systematic uncertainties in the line profile calculations, which could lead to differences between the temperature estimates from the continuum slope and the line profiles (Külebi et al. 2009). Regardless of these issues, we can safely conclude that J2211+1136 is a magnetic and mixed H/He atmosphere white dwarf with $M = 1.268 \pm 0.010\ M_\odot$, $\log g = 9.214 \pm 0.027$, and $T_{eff} \approx 7500$–8390 K.

3. J2255+0710 and J0103−0522

We acquired high-speed photometry of J2255+0710 and J0103−0522 right after we observed J2211+1136 on August 5 and September 9, respectively. We observed J2255+0710 over 45 minutes with 15 s long exposures, and J0103−0522 over 2 hr with 5 s long exposures. Figure 3 shows the APO light curves and Fourier transforms for both stars. Neither star shows any significant variability and we can rule out variability above 16.4 millimag in J2255+0710 and 5.4 millimag in J0103 −0522 at the 4⟨A⟩ level. Additional follow-up data on J2255 +0710 would be useful in pushing this detection limit down to lower amplitudes.

Out of the four magnetic ultramassive white dwarfs discussed in Kilic et al. (2021), two show photometric variability, J2211+1136 (discussed here) and J1901+1458 (Caiazzo et al. 2021). This fraction, 50%, is comparable to the
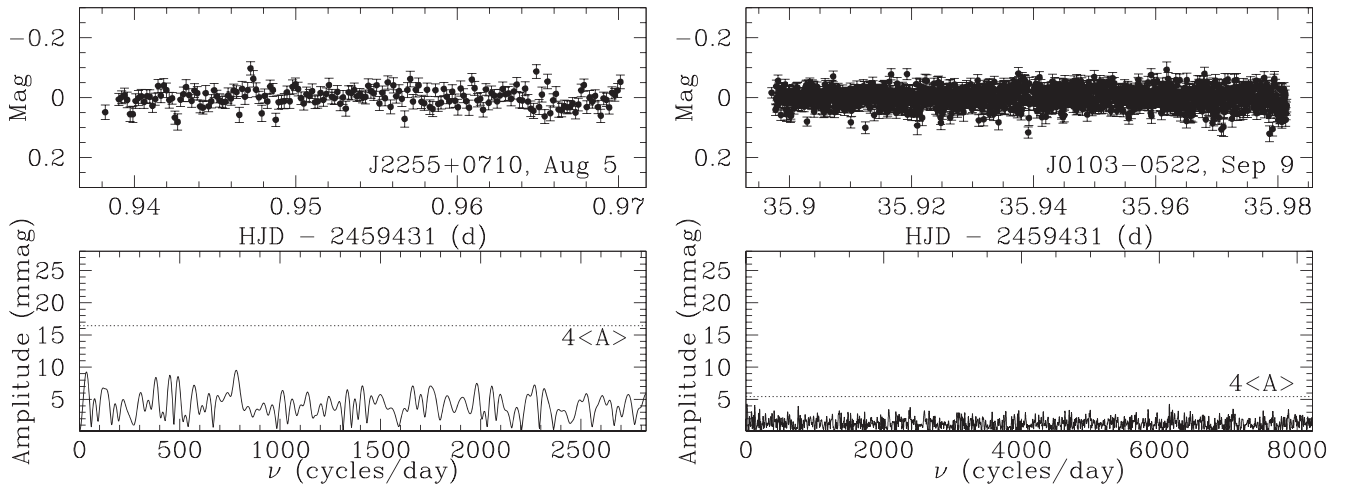
Figure 3. APO light curves of J2255 (top left) and J0103 (top right) obtained on UT 2021 August 5 and September 9, respectively. The bottom panels show the Fourier transform of these light curves, and 4 ⟨A⟩ levels.
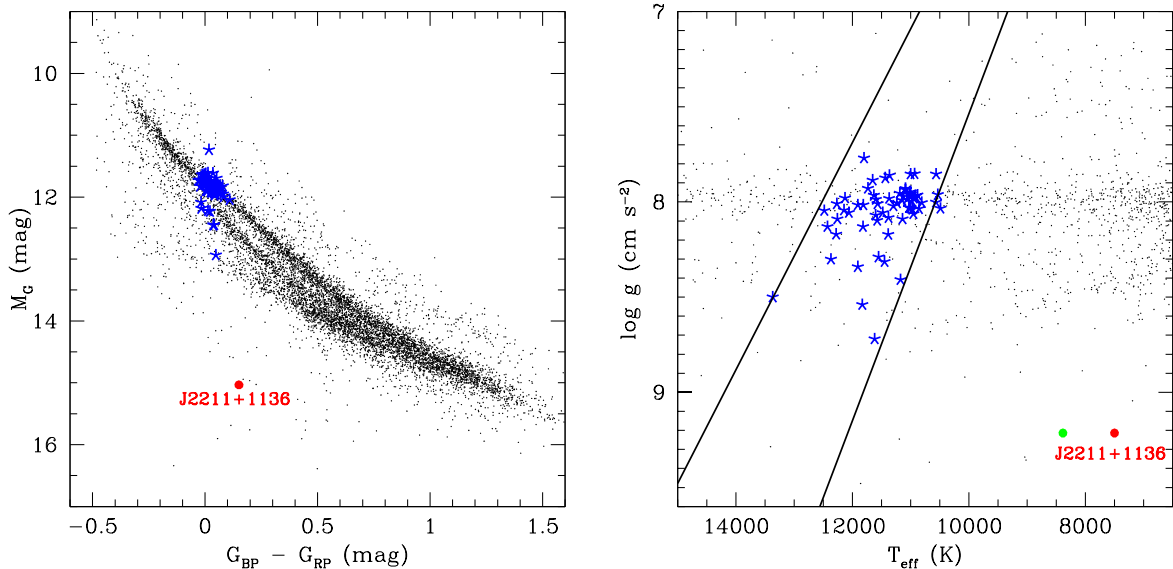

Figure 4. Left: Gaia color–magnitude diagram of the 100 pc sample in the Montreal White Dwarf Database (Dufour et al. 2017). Right: temperatures and surface gravities of the same stars. Blue stars mark the previously known pulsating DAV white dwarfs, and the solid lines mark the boundaries of the ZZ Ceti instability strip (Tremblay et al. 2015). The atmospheric parameters of J2211+1136 based on the photometric (green) and the spectroscopic (red) method are also shown. J2211 +1136 is clearly outside the boundaries of the instability strip.

67% fraction found in the larger variability survey of Brinkworth et al. (2013). Even though J2255+0710 and J0103 −0522 do not show large photometric variations, it is still possible that they could be fast rotators. For example, Kilic et al. (2019) detected significant changes in the Hα line profiles of G183-35 due to rotation, but G183-35 shows only low-level photometric variability, at 0.2%. Such a signal would be lost in the noise in our observations of J2255+0710 and J0103−0522.

4. Discussion

4.1. The Source of Variability in J2211+1136

There are two potential mechanisms to explain minute-scale variations in white dwarfs: pulsations and rotation. Figure 4 shows the ZZ Ceti instability strip for DA white dwarfs in color–magnitude and T_{eff}-log g space using the 100 pc MWDD white dwarf sample (Dufour et al. 2017). Blue stars mark the previously known pulsating DAV white dwarfs in that sample

and the solid lines show the empirical boundaries of the instability strip (see Tremblay et al. 2015, and references therein). The atmospheric parameters of J2211+1136 based on the photometric (green) and the spectroscopic (red, see Figure 2) method are also shown. J2211+1136 is significantly redder and cooler than the known pulsating DA white dwarfs and it is clearly outside the instability strip. The period of variability in J2211+1136 (70 s) is also significantly shorter than that in the shortest period ZZ Ceti pulsators (≈100 s).

Multiperiodicity is common among pulsating DAV white dwarfs (Mukadam et al. 2004; Fontaine & Brassard 2008; Winget & Kepler 2008). For example, BPM 37093 is a $T_{eff} = 11620 \pm 190$ K, $M = 1.13 \pm 0.10 \, M_{\odot}$ (assuming a CO core, Bédard et al. 2017) pulsating white dwarf that displays eight pulsation modes between 512 and 635 s (Metcalfe et al. 2004). Similarly, GD 518 is a $T_{eff} = 11420 \pm 110$ K, $M = 1.114 \pm 0.006 \, M_{\odot}$ (Kilic et al. 2020) pulsating white dwarf that displays multiperiodic luminosity variations at

timescales ranging from about 425 to 595 s (Hermes et al. 2013).

J2211+1136 is a He-rich DA white dwarf. It does not look like a ZZ Ceti star; it has a mixed H/He atmosphere and its surface temperature is too cool for pulsations. It also does not sound like a ZZ Ceti, it only shows monoperiodic variability. Hence, it certainly is not a pulsating white dwarf. The only other explanation for such short-period variability is the rotation of a spotted white dwarf.

4.2. The Fastest Spinning Isolated White Dwarf

Accreting white dwarfs in binary systems can be spun up to extremely fast rotation rates (e.g., Lopes de Oliveira et al. 2020), RX J0648.0−4418 being an excellent example with a spin period of 13.2 s (Mereghetti et al. 2021). However, isolated white dwarfs that go through single-star evolution rotate relatively slowly (Kawaler 2015; Hermes et al. 2017b).

Modeling the evolution of double white dwarf merger remnants, Schwab (2021) predicted rotation periods as short as 5 minutes for the most massive white dwarfs with $M \gtrsim 1.2\,M_\odot$. They also found that increasing mass ratio (at fixed total mass) leads to higher final masses and shorter periods and concluded that a rotation period of ∼10 minutes in a single white dwarf is a signature of its merger origin.

Prior to the discovery observations presented here, the fastest spinning isolated white dwarfs had rotation periods of ≈5 minutes (Williams et al. 2016; Kawka 2020; Pshirkov et al. 2020; Reding et al. 2020; Caiazzo et al. 2021). With a rotation rate of $P = 70.32 \pm 0.04$ s, J2211+1136 becomes the fastest spinning isolated white dwarf known. In addition to its fast rotation, J2211+1136 is strongly magnetic, massive, an outlier in its transverse velocity, and also an outlier in its atmospheric composition (see Figure 8 in Rolland et al. 2018). Hence, J2211+1136 presents all of the symptoms of being a double white dwarf merger product.

4.3. Fast-spinning White Dwarfs Impersonating ZZ Cetis

Pure-hydrogen-atmosphere white dwarfs are expected to enter the ZZ Ceti instability strip once they cool down to about 12,000 K (for average $0.6\,M_\odot$ white dwarfs, Fontaine & Brassard 2008; Winget & Kepler 2008). These nonradial *g*-mode pulsations have periods ranging from 100 to 2000 s. The purity of the ZZ Ceti instability strip has been discussed at length by Mukadam et al. (2004) and Vincent et al. (2020). It is expected that every pure-hydrogen-atmosphere white dwarf passing through the instability strip during their evolution should pulsate. However, the presence of a magnetic field may significantly affect the pulsation-driving mechanism (Tremblay et al. 2015). The case of WD 2105−820 is especially interesting; a ∼56 kG field seems to be sufficient to suppress atmospheric convection (Gentile Fusillo et al. 2018) and therefore inhibit pulsations. This suggests that magnetic white dwarfs should not pulsate, even if they are within the confines of the instability strip (Vincent et al. 2020).

The presence of magnetic white dwarfs within the instability strip implies that some of them will show monoperiodic photometric variations due to rotation. Such fast-rotating magnetic white dwarfs can impersonate a pulsating ZZ Ceti star. For example, Kilic et al. (2015) discovered photometric variations in a massive DA white dwarf, J1529+292, that is very close to the red edge of the instability strip. However,

given the relatively long period of 38 minutes, they ruled out pulsations as the source of variability and instead suggested a spotted white dwarf. If the rotation period of J1529+2928 was less than about 20 minutes, it would have been classified as a ZZ Ceti. Curd et al. (2017) identified four massive pulsating DA white dwarfs, but three of them show monoperiodic variability, even though monoperiodic pulsators are rare (e.g., Mukadam et al. 2004; Hermes et al. 2017b). Unless higher signal-to-noise ratio observations detect additional pulsation modes, it is difficult to confirm these monoperiodic variables as pulsating DAVs.

5. Conclusions and Future Directions

We presented follow-up time-series photometry of three ultramassive white dwarfs in the 100 pc sample (Kilic et al. 2021) and reported the discovery of 70.3 s photometric variations in one of these systems. J2211+1136 becomes the fastest spinning isolated white dwarf known. J2211+1136 shows all of the signatures of a binary merger outcome; it is strongly magnetic, a fast rotator, ultramassive, and has a relatively large transverse velocity and an unusual atmospheric composition.

Briggs et al. (2015) suggested that binary mergers could explain the incidence of magnetism and the mass distribution of highly magnetic white dwarfs. Since mergers also lead to fast rotation rates (Schwab 2021), it is natural to expect a trend in mass and rotation. So far, only a small fraction of the ultramassive white dwarfs in the solar neighborhood have spectral classification available. Additional follow-up spectroscopy and high-speed photometry would be useful to search for additional magnetic white dwarfs and fast rotators and search for trends between the rotation rates and other physical parameters of these objects (Brinkworth et al. 2013; Hermes et al. 2017b).

Large-scale photometric surveys like the ZTF (Bellm et al. 2019) and the Vera Rubin Observatory's Legacy Survey of Space and Time (LSST) will provide an unprecedented opportunity to enlarge the sample of spotted white dwarfs with rotation measurements (e.g., Caiazzo et al. 2021). As an example, a quick search of the ZTF photometry for the ultramassive white dwarfs presented in Kilic et al. (2021) shows significant variability for WD J070753.00+561200.25 with a 63 minute period. Expanding this search to the (candidate) magnetic white dwarfs with $M \geqslant 1\,M_\odot$ in the 100 pc SDSS sample of Kilic et al. (2020) reveals four additional variables, SDSS J011810.32−015612.3, J071816.40+373139.0, J103941.52−032534.2, and J154315.09 +302133.5. There are many other fast-rotating magnetic white dwarfs waiting to be discovered in the ZTF (I. Caiazzo 2021, private communication), and eventually in the LSST.

The existence of fast-rotating white dwarfs outside of the ZZ Ceti strip indicates that there must be some within the strip. Such monoperiodic variability can be easily confused with nonradial *g*-mode pulsations. Since a large fraction of massive white dwarfs form through mergers (Temmink et al. 2020) and such remnants are also likely to be fast-spinning magnetic white dwarfs (Briggs et al. 2015; Schwab 2021), we would expect the fraction of ZZ Ceti impostors to be larger for more massive white dwarfs. Separating the true pulsators from the ZZ Ceti impostors would require the detection of multiperiodic variations (for ZZ Cetis) or a magnetic field (for the impostors) through high-resolution spectroscopy or spectropolarimetry.

Fast-rotating white dwarfs with photometric variations provide an excellent clock to time the system. Stellar pulsations have been used to search for planetary companions around

white dwarfs (Winget et al. 2003; Mullally et al. 2008), but stable pulsation modes are essential for a successful search (Hermes 2013). The timing method works best for stars with high-amplitude, short-period oscillations that are stable.

Timing measurements of millisecond pulsars identified the first planetary objects outside of the solar system (Wolszczan 1994). J2211+1136 and other fast-spinning isolated white dwarfs with significant photometric variability (e.g., Williams et al. 2016; Kawka 2020; Pshirkov et al. 2020; Reding et al. 2020; Caiazzo et al. 2021) open a new discovery space for similar objects around white dwarfs. Long-term monitoring of the spin evolution of these isolated white dwarfs can provide meaningful constraints on the occurrence rate of substellar and planetary mass companions around their progenitor systems.

ORCID iDs

Mukremin Kilic ◉ https://orcid.org/0000-0001-6098-2235
Alekzander Kosakowski ◉ https://orcid.org/0000-0002-9878-1647
Adam G. Moss ◉ https://orcid.org/0000-0001-7143-0890
P. Bergeron ◉ https://orcid.org/0000-0003-2368-345X
Annamarie A. Conly ◉ https://orcid.org/0000-0002-2545-3597

References

Bédard, A., Bergeron, P., & Fontaine, G. 2017, ApJ, 848, 11
Bellm, E. C., Kulkarni, S. R., Graham, M. J., et al. 2019, PASP, 131, 018002
Bergeron, P., Ruiz, M.-T., & Leggett, S. K. 1992, ApJ, 400, 315
Bergeron, P., Ruiz, M. T., & Leggett, S. K. 1997, ApJS, 108, 339
Bergeron, P., Wesemael, F., & Fontaine, G. 1991, ApJ, 367, 253
Briggs, G. P., Ferrario, L., Tout, C. A., Wickramasinghe, D. T., & Hurley, J. R. 2015, MNRAS, 447, 1713
Brinkworth, C. S., Burleigh, M. R., Lawrie, K., Marsh, T. R., & Knigge, C. 2013, ApJ, 773, 47
Caiazzo, I., Burdge, K. B., Fuller, J., et al. 2021, Natur, 595, 39
Coutu, S., Dufour, P., Bergeron, P., et al. 2019, ApJ, 885, 74
Curd, B., Gianninas, A., Bell, K. J., et al. 2017, MNRAS, 468, 239
Dufour, P., Béland, S., Fontaine, G., Chayer, P., & Bergeron, P. 2011, ApJL, 733, L19
Dufour, P., Blouin, S., Coutu, S., et al. 2017, in ASP Conf. Ser. 509, 20th European White Dwarf Workshop, ed. P. E. Tremblay, B. Gaensicke, & T. Marsh (San Francisco: ASP), 3

Dunlap, B. H., & Clemens, J. C. 2015, in ASP Conf. Ser. 493, 19th European Workshop on White Dwarfs, ed. P. Dufour, P. Bergeron, & G. Fontaine (San Francisco: ASP), 547
Ferrario, L., Wickramasinghe, D., & Kawka, A. 2020, AdSpR, 66, 1025
Fontaine, G., & Brassard, P. 2008, PASP, 120, 1043
Gentile Fusillo, N. P., Tremblay, P. E., Jordan, S., et al. 2018, MNRAS, 473, 3693
Hermes, J. J. 2013, BAAS, 221, 424.04
Hermes, J. J., Kawaler, S. D., Romero, A. D., et al. 2017a, ApJL, 841, L2
Hermes, J. J., Kepler, S. O., Castanheira, B. G., et al. 2013, ApJL, 771, L2
Hermes, J. J., Gänsicke, B. T., Kawaler, S. D., et al. 2017b, ApJS, 232, 23
Kawaler, S. D. 2004, in Proc. of IAU Symposium 215, Stellar Rotation, ed. A. Maeder & P. Eenens (San Francisco: ASP), 561
Kawaler, S. D. 2015, in ASP Conf. Ser. 493, 19th European Workshop on White Dwarfs, ed. P. Dufour, P. Bergeron, & G. Fontaine (San Francisco: ASP), 65
Kawka, A. 2020, in Proc. of IAU 357, White Dwarfs as Probes of Fundamental Physics: Tracers of Planetary, Stellar and Galactic Evolution, ed. M. A. Barstow et al. (Dordrecht: Reidel), 60
Kemic, S. B. 1974, JILA 1153, 113, 1
Kilic, M., Bergeron, P., Blouin, S., & Bédard, A. 2021, MNRAS, 503, 5397
Kilic, M., Bergeron, P., Dame, K., et al. 2019, MNRAS, 482, 965
Kilic, M., Bergeron, P., Kosakowski, A., et al. 2020, ApJ, 898, 84
Kilic, M., Gianninas, A., Bell, K. J., et al. 2015, ApJL, 814, L31
Koester, D., Dreizler, S., Weidemann, V., & Allard, N. F. 1998, A&A, 338, 612
Külebi, B., Jordan, S., Euchner, F., Gänsicke, B. T., & Hirsch, H. 2009, A&A, 506, 1341
Lopes de Oliveira, R., Bruch, A., Rodrigues, C. V., Oliveira, A. S., & Mukai, K. 2020, ApJL, 898, L40
Mereghetti, S., Pintore, F., Rauch, T., et al. 2021, MNRAS, 504, 920
Metcalfe, T. S., Montgomery, M. H., & Kanaan, A. 2004, ApJL, 605, L133
Montgomery, M. H., Williams, K. A., Winget, D. E., et al. 2008, ApJL, 678, L51
Mukadam, A. S., Mullally, F., Nather, R. E., et al. 2004, ApJ, 607, 982
Mullally, F., Winget, D. E., Degennaro, S., et al. 2008, ApJ, 676, 573
Pshirkov, M. S., Dodin, A. V., Belinski, A. A., et al. 2020, MNRAS, 499, L21
Reding, J. S., Hermes, J. J., Vanderbosch, Z., et al. 2020, ApJ, 894, 19
Rolland, B., & Bergeron, P. 2015, in ASP Conf. Ser. 493, 19th European Workshop on White Dwarfs, ed. P. Dufour, P. Bergeron, & G. Fontaine (San Francisco: ASP), 53
Rolland, B., Bergeron, P., & Fontaine, G. 2018, ApJ, 857, 56
Schwab, J. 2021, ApJ, 906, 53
Tayar, J., & Pinsonneault, M. H. 2013, ApJL, 775, L1
Temmink, K. D., Toonen, S., Zapartas, E., Justham, S., & Gänsicke, B. T. 2020, A&A, 636, A31
Tremblay, P. E., Gianninas, A., Kilic, M., et al. 2015, ApJ, 809, 148
Tremblay, P. E., Hollands, M. A., Gentile Fusillo, N. P., et al. 2020, MNRAS, 497, 130
Vincent, O., Bergeron, P., & Lafrenière, D. 2020, AJ, 160, 252
Williams, K. A., Montgomery, M. H., Winget, D. E., Falcon, R. E., & Bierwagen, M. 2016, ApJ, 817, 27
Winget, D. E., Cochran, W. D., Endl, M., et al. 2003, in ASP Conf. Ser. 294, Scientific Frontiers in Research on Extra Planets, ed. D. Deming & S. Seager (San Francisco: ASP), 59
Winget, D. E., & Kepler, S. O. 2008, ARA&A, 46, 157
Wolszczan, A. 1994, Sci, 264, 538